Kinetics of Myosin Node Aggregation into a Contractile Ring

Nikola Ojkic and Dimitrios Vavylonis*

Department of Physics, Lehigh University, Bethlehem Pennsylvania 18015, USA

(Received 18 January 2010; published 20 July 2010)

We study a stochastic aggregation model for the assembly of the contractile ring from a broad band of nodes during cytokinesis in fission yeast. We found that bands of nodes condense into rings when the range of node interactions is larger than the width of the band. Wide bands are unstable to clump formation due to Poisson density fluctuations. We derive expressions for node kinetics and times for ring vs clump formation and test them using numerical simulations. These results suggest clump formation mechanisms in mutant cells.

DOI: 10.1103/PhysRevLett.105.048102 PACS numbers: 87.16.A−, 87.16.Ka, 87.17.Ee

The ability of eukaryotic cells to move and change shape relies on the plasticity of the cellular cytoskeleton. The components of the cytoskeleton (actin, tubulin, molecular motors) spontaneously come together to generate filamentous structures over scales much larger than the size of individual proteins. Understanding the physics that govern the assembly of these adaptive meshworks is an area of considerable research [1–6]. One of the best examples of such a subcellular self-organization process is the assembly of the actomyosin contractile ring during cytokinesis [7–10], the last step of cell division. A model organism for cytokinesis is fission yeast [11–14], where the contractile ring forms through the condensation of a broad band of ~65 "nodes" [9,15,16]. The nodes are macromolecular complexes bound to the inner part of the cell membrane and contain myosin-II, actin filament nucleator formin Cdc12p, scaffolding protein Mid1p, and F-BAR domain-containing Cdc15p [13,17]. During mitosis, nodes assemble in the middle of the yeast cell over a broad band, 1.8 μm in width, that condenses into a ring within ~10 min; see Fig. 1(a).

A proposed mechanism by which nodes condense into a ring is "search, capture, pull, and release" (SCPR) [9] [see Fig. 1(c)]. In this model, Cdc12p nucleates actin filaments that polymerize out of nodes. These filaments grow along random directions parallel to the cell membrane. When the tip of an elongating filament comes in close vicinity of a target node, an actomyosin connection is established. Once connected, the myosin motors at the target exert forces that pull the pair of nodes toward one another. Myosin may depolymerize actin as it slides along the filament [3] and reduce Cdc12p-mediated actin elongation through tension [9]. Actin filament severing protein cofilin breaks up connections, allowing nodes to reinitiate actin elongation along a new direction [9].

Simulations of the 2D SCPR model generated rings consistently with experiment [Fig. 1(a)]. However, for parameter values different than those seen in experiment, the model generated disconnected clumps [9]. Recently, Hachet and Simanis [18] observed node clump formation in cells with mutations in node proteins such as Cdc12p [see Fig. 1(b)]. To better understand the mechanism of clump vs ring formation, here we present analytical and numerical results of a stochastic node aggregation model. In the model, nodes with attached myosin form clumps through connections by filaments of varying length. This

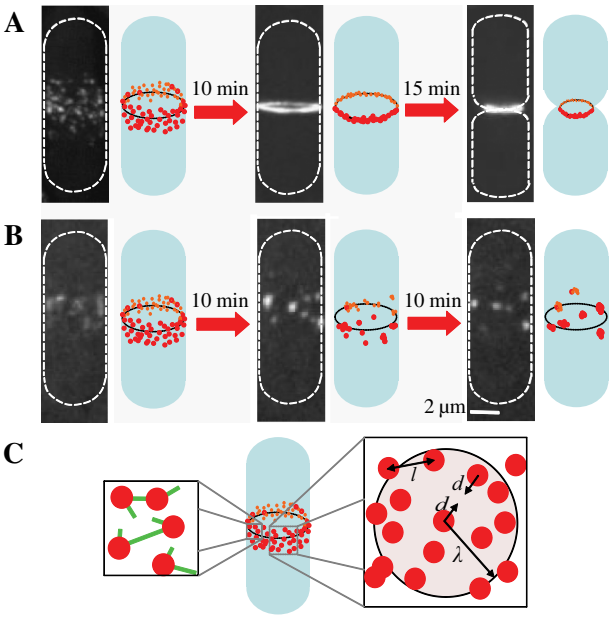

FIG. 1 (color online). Formation of contractile ring by aggregation of broad band of nodes. (A) Images of dividing wild-type cells expressing myosin marker Rlc1p-3GFP [9]. A broad band of nodes bound in the inner part of the cell membrane condenses into a ring in ~10 minutes. The ring subsequently constricts. (B) Images of mitotic *cdc12p-112* cells (formin mutants) expressing Rlc1p-GFP at the restrictive temperature: clumps form instead of rings [18]. (C) 2D stochastic aggregation model. Left: nodes attract one another through transient connections by actin filaments polymerized by formins at the nodes. Right: model parameters. l, average distance between neighboring nodes; d, size of pairwise node movement per connection event; and λ, typical length of actin filaments.

mechanism differs from previous studies in which filaments collapse into bundles through mobile motors [1–6].

We consider the model of Fig. 1(c) in which each node on a 2D surface representing the inner cell membrane can establish a connection with another node at a distance r away with rate $q(r) = Q(a/r)e^{-r/\lambda}$. Here, the $1/r$ dependence reflects the diluteness in the search process as the actin filaments grow out of Cdc12p nucleators in the nodes, Q is a rate that depends on total number of Cdc12p per node, and the exponential term introduces an upper cutoff of order λ representing the typical length at which actin filaments grow before severing by cofilin. Parameter a is a capture radius: it represents the distance over which the tips of the growing actin filaments are captured by target nodes [9]. Myosin pulling and severing of connections is modeled as follows. When a connection between two nodes is established, the nodes move toward one another by distance d instantaneously (when $r < 2d$, they are moved by $r/2$ such that they overlap). After this movement, the connection is assumed broken. For simplicity, excluded volume interactions are neglected.

The model of Fig. 1(c) combines two types of node movement: (i) active diffusion due to the randomness in connections with neighbors (described by a diffusion coefficient, D), and (ii) directed transport towards regions of higher density with local velocity v. Monte Carlo simulations showed that active diffusion is not strong enough to maintain an initially homogeneous 2D state of nodes at concentration c. Plots of the mean square node displacement vs time indicate that an initial diffusive $t^{1/2}$ regime is followed by directed transport and clump formation [see Fig. 2]. The following scaling arguments that neglect numerical prefactors describe the kinetics of clump formation observed in simulations.

In a homogeneous 2D system, clumps form near regions that happen to have a higher density initially due to Poisson fluctuations around the average concentration. Consider a node at $t = 0$. Since the step size of the node's walk is d, its initial diffusion coefficient is

$$D_0 \approx Q_{\rm tot} d^2, \qquad Q_{\rm tot} \equiv \int_0^\infty c q(r) 2\pi r dr \approx Q\frac{a\lambda}{l^2}. \quad (1)$$

Here $Q_{\rm tot}$ is the total rate of making connections to other nodes and $l \equiv c^{-1/2}$ is the typical distance between neighboring nodes [see Fig. 1(c)]. Note that most connections are made at distance of order λ since the integral in Eq. (1) is dominated by $r \sim \lambda$. Thus a node can connect with approximately $N_\lambda \equiv \lambda^2/l^2$ nodes at distance of order λ. The initial Poisson fluctuations in the number of nodes over such a distance is $\Delta N_\lambda = N_\lambda^{1/2} = \lambda/l$. Therefore, initially, there is a direction in space along which the node is attracted to by an excess of ΔN_λ nodes. The node will move along this direction with an initial velocity:

$$v_0 \approx Q' d \Delta N_\lambda = Q' d\lambda/l, \qquad Q' \equiv Qa/\lambda, \quad (2)$$

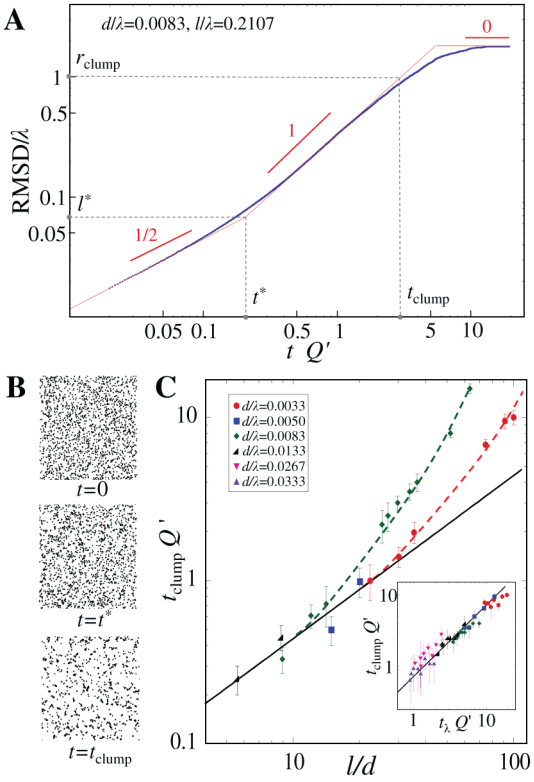

FIG. 2 (color online). Monte Carlo simulations of node aggregation showing kinetics of clump formation in Regime 1 ($d \ll l \ll \lambda$). Nodes were placed according to a 2D uniform probability distribution. $q(r)$ was set to zero for $r > 3\lambda$. Periodic boundary conditions were used. (A) RMS displacement vs time. Slope 1/2 regime: active diffusion up to t^*; slope 1 regime: clump formation that ends at $t_{\rm clump}$; slope 0 regime: nodes trapped in isolated clumps. (B) Snapshots of node configurations at different times. (C) Test of $t_{\rm clump}Q' \approx l/d$, Eq. (4). $t_{\rm clump}$ is the time at which the slope of the linear regime in A decreases by 20% ±10%. Solid (black) line: $t_{\rm clump}Q' = 0.044(6)l/d$ is a linear fit to the subset of the data most asymptotic in R1. Dashed lines are guide-to-the-eye curves indicating approach to common asymptotic regime; deviations occur for l approaching λ. Inset shows $t_{\rm clump} = 0.73(3)t_\lambda$, in agreement with Eq. (4).

where Q' is the connection rate for nodes separated by distance λ. The expressions in Eqs. (1) and (2) define a length scale l^* and time t^* after which transport dominates diffusion, $l^* = v_0 t^* = (D_0 t^*)^{1/2}$ [19]

$$l^* = \lambda d/l, \qquad t^* = 1/Q'. \quad (3)$$

There are two asymptotic limits: (1) Regime 1 (R1): $d \ll l$, or, equivalently, $l^* \ll \lambda$, and (2) Regime 2 (R2): $d \gg l$ ($l^* \gg \lambda$). Throughout, we consider $d \ll \lambda$ and $l \ll \lambda$.

For R1, active diffusion is not strong enough to move nodes over distances beyond their interaction range. Thus, nodes continue to move and coalesce with speed v_0 according to the initial concentration fluctuations past t^*. This linear transport of nodes persists until nodes travel a distance of order λ; at about this point in time, regions of

high initial density absorb the nodes of the less dense regions [see Fig. 2(b)]. As a result, denser regions of size λ separate from regions depleted of nodes of the same size and form clumps separated from one another by r_{clump} over a time t_{clump}, where

$$r_{\mathrm{clump}} \approx \lambda, \quad t_{\mathrm{clump}} \approx \lambda/v_0 \approx l/(Q'd) \quad (\mathrm{R1}, d \ll l). \quad (4)$$

These isolated clumps subsequently self-collapse rapidly: as the interaction of nodes with their neighbors that segregate into different clumps is lost, clumps condense into spots over a time much shorter than t_{clump}. We tested this scaling expression for t_{clump} in Fig. 2. We also tested $r_{\mathrm{clump}} \approx \lambda$ by showing that $t_{\mathrm{clump}} \approx t_\lambda$ numerically, where t_λ is the time when the root mean square displacement (RMSD) reaches λ.

For R2, active diffusion is strong: nodes travel distances $L(t)$ larger than the interaction range λ [see Fig. 3(a)]. This leads to different kinetics. As nodes get displaced over $L(t) > \lambda$, the diffusion coefficient remains unchanged from Eq. (1). However, nodes experience an increasingly larger transport rate v_t due to Poisson fluctuations over distances $L(t)$. Since 2D diffusion is marginally compact [20], nodes sample their exploration volume uniformly, within logarithmic corrections. Thus, replacing λ by $L(t)$ in Eq. (2):

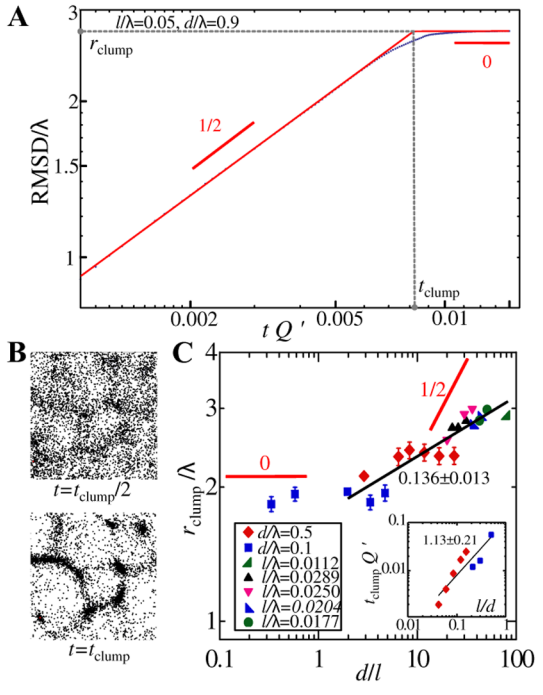

FIG. 3 (color online). Simulations as in Fig. 1, but for Regime 2 ($l \ll d \ll \lambda$). (A) RMS displacement vs time. Slope 1/2 regime: active diffusion; slope 0 regime: nodes trapped in clumps. (B) Snapshots of node configurations. (C) Test of Eq. (6). Thick (red) lines show predicted slopes in R1, R2; thin (black) lines show fits. t_{clump} is time required to reach RMSD plateau (panel A) and r_{clump} is corresponding distance.

$$v_t \approx Q' dL(t)/l. \quad (5)$$

The distance at which transport by v_t dominates diffusion marks the time at which clumps start to form, $r_{\mathrm{clump}} = v_{t_{\mathrm{clump}}} t_{\mathrm{clump}} = (D_0 t_{\mathrm{clump}})^{1/2}$. This gives

$$r_{\mathrm{clump}} \approx \lambda (d/l)^{1/2}, \qquad t_{\mathrm{clump}} \approx l/(Q'd) \qquad (\mathrm{R2}, d \gg l). \quad (6)$$

The simulations of Fig. 3(a) verify that, unlike Fig. 2(a), there is no intermediate linear regime: once transport dominates diffusion at t_{clump}, groups of nodes within $r_{\mathrm{clump}} = L(t_{\mathrm{clump}})$ of one another collapse rapidly into isolated clusters; see Fig. 3(b). The scaling of t_{clump} in Fig. 3(c) is consistent with Eq. (6). The exponent of r_{clump} in Fig. 3(c) differs from 1/2, possibly due to a slow crossover from R1 (slope 0), logarithmic terms, or unaccounted many-body correlations that develop over time. Further numerical tests, deeper in R2, were prohibited by the large number of nodes required ($>10^7$).

The above results describe a bulk system. Consider now a 2D *band* of nodes of width w. The following arguments agree with simulations in Fig. 4. Because of concentration gradients, nodes at distances of order w from the middle of the band experience directed transport towards the center with velocity $v_w \approx \int_{-\pi}^{\pi} \int_0^{\infty} c(r, \phi) q(r) d \cos\phi dr d\phi$. This integral is over a radial coordinate system centered at a node, $c(r, \phi)$ is node concentration, and $d\cos\phi$ is distance traveled towards the center for connections at angle ϕ. The integral is dominated by r of order the smallest of w and λ:

$$v_w \approx \begin{cases} Qadcw, & w \ll \lambda \\ Qadc\lambda^2/w, & w \gg \lambda, \end{cases} \quad (7)$$

assuming that the typical gradient across the band is of order c/w, where c is concentration in the middle.

For narrow bands, $w \ll \lambda$, the velocity v_w defines a time over which boundary nodes travel distance w:

$$t_{\mathrm{shrink}} \equiv w/v_w \approx l^2/(Qad) \qquad (w \ll \lambda). \quad (8)$$

This time is *shorter* than t_{clump}, for both R1 and R2, since $t_{\mathrm{shrink}}/t_{\mathrm{clump}} = l/\lambda \ll 1$, using Eqs. (4) and (6). Thus, narrow bands condense ("shrink") into rings *before* clumps have sufficient time to form.

Wide bands, $w \gg \lambda$, do not condense into rings. In this case, $t_{\mathrm{shrink}} \approx w^2 l^2/(Qad\lambda^2)$. There are two subcases. (i) For very wide bands, $w \gg \lambda(\lambda/l)^{1/2}$, $t_{\mathrm{clump}} \ll t_{\mathrm{shrink}}$, using Eqs. (4) and (6). Therefore, clumps form before the band condenses. (ii) Bands with $\lambda \ll w \ll \lambda(\lambda/l)^{1/2}$ split into smaller bands over a time of order t_{shrink}. To see this, consider two nodes within interaction range, i.e., within λ of one another. Because of the density gradient, the difference in their condensation velocities toward the middle is of order $\Delta v_\lambda \approx Qad\lambda^2 \Delta c_\lambda / w$, where $\Delta c_\lambda \approx c\lambda/w$. These nodes lose contact with one another when their relative velocity transports them over distances of order

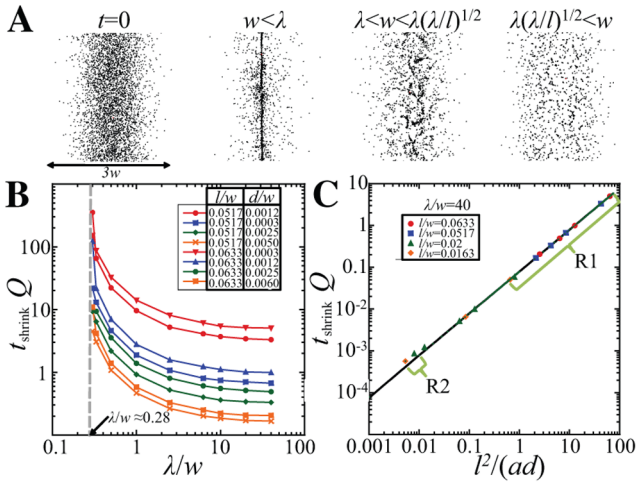

FIG. 4 (color online). Simulations of condensation of a band of nodes (periodic boundary conditions vertically). Nodes were placed according to Gaussian distribution with variance $w/2$. (A) Initial distribution (first panel) and snapshots of successful condensation or clump formation for different λ ($l/w = 0.0315$, $d/w = 0.0125$, $a/w = 0.25$). (B) Condensation time (time required for the standard deviation to decrease by $1/2$) vs λ/w using $a/w = 0.25$. For $\lambda/w < 0.28$ the band does not shrink. (C) Test of $t_{\text{shrink}} \approx l^2/(Qad)$. Solid (black) line is linear fit to R1 data: $t_{\text{shrink}} = 0.078(5)l^2/(Qad)$.

λ. This occurs over time $t_{\text{split}} = \lambda/\Delta v_\lambda \approx t_{\text{shrink}}$ causing the band to lose internal connectivity as it is about to form a ring [see Fig. 4(a)].

Let us apply the above results to fission yeast, using parameter values obtained from prior experiments [9,15]: $d = 0.45\ \mu$m, $l = 0.77\ \mu$m, $w = 1.8\ \mu$m, $a = 0.1\ \mu$m, $1/Q = 0.67$ min, and $\lambda = 1\ \mu$m. These values are near the R1-R2 boundary. Since $\lambda/w = 0.56$, the band is just narrow enough to allow condensation. Simulations using these values indicate $t_{\text{shrink}} = 15$ min [13 min using Eq. (8)], very close to experiments; see Fig. 1. For a 2D bulk of nodes we find $t_{\text{clump}} = 15$ min with simulations [12 min using Eq. (4)]. We suggest that the small difference in these two times leads to clump formation in *cdc12-112* mutants in Fig. 1: a small change in the polymerization rate of actin, for example, may result in slightly shorter actin filaments causing the cell to shift to the $\lambda < 0.28w$ regime of Fig. 4(c). Since Cdc15p recruits Cdc12p to the nodes, and since the septation initiation network pathway promotes proper Cdc15p localization, we suggest that a similar mechanism explains clump formation in Cdc15p and septation initiation network pathway mutants [18]. Image analysis of actin in these cells [11,15] could test this prediction. Another prediction of the model is the formation of fragmented linear structures for intermediate values of λ [Fig. 4(a)].

Cells may have optimized parameter values. Presumably, the width of the node band is limited by the accuracy with which cells locate their middle [21]. We speculate that yeast establishes filaments long enough ($\lambda \sim w$) to achieve condensation without clumps, but not much longer; the latter would provide little benefit since the condensation time is independent of λ, to leading order. Condensation is accelerated by smaller l (high node densities); thus, the number of nodes may reflect the balance between speed and cost required to generate nodes. Additionally, the condensation time decreases with increasing node step d, whose upper limit is $\sim\lambda/2$. This could be the reason why $d/\lambda \approx 0.5$ in cells.

Future work is required to explore the following: (i) In Eq. (1), the total connection rate increases with concentration, though in reality it is limited by the number of formins per node. This saturation can be accounted for using a density-dependent Q. (ii) Connections between nodes in close proximity "screen" long connections; thus, λ depends on node concentration. (iii) Fluctuations in the number of myosins per node could enhance clump instabilities. (iv) Additional mechanisms, such as cross-linking, may stabilize aligned nodes and contribute to ring formation in cells with defective nodes [14,18].

We thank Matt Smith for help with simulations. This work was supported by NIH Grant No. R21GM083928.

*vavylonis@lehigh.edu

[1] G. H. Koenderink *et al.*, Proc. Natl. Acad. Sci. U.S.A. **106**, 15192 (2009).
[2] R. Chelakkot, R. Lipowsky, and T. Gruhn, Soft Matter **5**, 1504 (2009).
[3] L. Haviv *et al.*, J. Mol. Biol. **375**, 325 (2008).
[4] F. Ziebert, I. S. Aranson, and L. S. Tsimring, New J. Phys. **9**, 421 (2007).
[5] K. Kruse *et al.*, Phys. Rev. Lett. **92**, 078101 (2004).
[6] T. B. Liverpool and M. C. Marchetti, Phys. Rev. Lett. **90**, 138102 (2003).
[7] A. Zumdieck *et al.*, Phys. Rev. Lett. **95**, 258103 (2005).
[8] R. Shlomovitz and N. S. Gov, Biophys. J. **94**, 1155 (2008).
[9] D. Vavylonis *et al.*, Science **319**, 97 (2008).
[10] G. Salbreux, J. Prost, and J. F. Joanny, Phys. Rev. Lett. **103**, 058102 (2009).
[11] R. Arai and I. Mabuchi, J. Cell Sci. **115**, 887 (2002).
[12] R. R. Daga and F. Chang, Proc. Natl. Acad. Sci. U.S.A. **102**, 8228 (2005).
[13] J.-Q. Wu *et al.*, J. Cell Biol. **174**, 391 (2006).
[14] Y. Huang, H. Yan, and M. K. Balasubramanian, J. Cell Biol. **183**, 979 (2008).
[15] V. C. Coffman *et al.*, Mol. Biol. Cell **20**, 5195 (2009).
[16] T. Drake and D. Vavylonis, HFSP J. **4**, 122 (2010).
[17] J.-Q. Wu and T. D. Pollard, Science **310**, 310 (2005).
[18] O. Hachet and V. Simanis, Genes Dev. **22**, 3205 (2008).
[19] B. O'Shaughnessy and D. Vavylonis, Phys. Rev. Lett. **90**, 118301 (2003).
[20] P. G. de Gennes, J. Chem. Phys. **76**, 3316 (1982).
[21] F. Tostevin, P. R. ten Wolde, and M. Howard, PLoS Comput. Biol. **3**, e78 (2007).